PAPER

Check for updates

pH-Sensitive magnetite mesoporous silica nanocomposites for controlled drug delivery and hyperthermia†

Hasan Keshavarz, [ID] [a] Alireza Khavandi,[a] Somaye Alamolhoda [ID] *[a] and M. Reza Naimi-Jamal [ID] [b]

In clinical applications, chemotherapy and hyperthermia are commonly used together. To achieve this, we synthesized multifunctional magnetite mesoporous silica nanoparticles (MMSNs) coated with a chitosan hydrogel. pH-Responsive chitosan hydrogels (cross-linked glutaraldehyde) were used to cover mesoporous silica pores. The infrared spectroscopy (FT-IR) and electron microscopy images (SEM and TEM) confirm that a hydrogel layer and a silica shell were formed. By applying alternating magnetic fields (AMF) to nanogels, heat generation (43 °C) occurred within a short time. The drug release (tamoxifen) of nanogels was studied for 72 h at different pH and temperatures. Drug release at pH 7.4/$T = 37$ °C (simulating physiological condition) and pH 5/$T = 43$ °C (pH simulating endosomes/hyperthermia) were 15 and 70%, respectively, so, drug release was increased with hyperthermia. To determine the biocompatibility of the nanogels, an MTT assay of L929 cells was performed for 24, 48 and 72 h. The results show high biocompatibility of nanogels even at high concentrations (over 80% cell viability after 72 h for all concentrations).

## 1. Introduction

Nanotechnology has made significant advances in various fields such as drug delivery. Chemotherapy is one of the common ways to control and treat cancer. Chemotherapy drugs are usually highly toxic and their use can cause various side effects for patients, such as hair loss and nausea. Magnetic nanoparticles are one of the attractive options for delivery of drug molecules because by applying an external magnetic field the nanoparticles can be transferred directly to the target tissue. Among the benefits of using targeted magnetic systems are reducing the side effects of the toxic drug, reducing the need for drug use and reducing treatment costs.[1–3]

Magnetic nanoparticles with different nuclei are used, such as MFe_2O_4 (M = Co, Mn and Zn) and iron oxides (such as magnetite and maghemite). Mn, Co cores are not widely considered due to their intrinsic toxicity. Superparamagnetic iron oxide nanoparticles (SPIONs) especially magnetite nanoparticles are very popular for biomedical applications.[1,4] The

most common method for the synthesis of these particles is co-precipitation of iron salts (Fe^{2+} and Fe^{3+}) as follows:[5]

$$Fe^{2+} + 2Fe^{3+} + 8OH^- \rightarrow Fe_3O_4 + 4H_2O \quad (1)$$
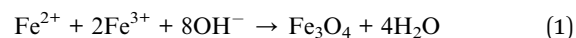
Surface modification of SPIONs nanoparticles could improve their biocompatibility for use in biomedical applications. Coating of magnetite nanoparticles can: prevent agglomeration of nanoparticles, increase biocompatibility, increase the time of circulation of nanoparticles in the body and prevent oxidation of magnetite nanoparticles. Mesoporous silica is one of the most attractive coatings for biomedical applications. Advantages of silica shell:[6,7]

■ Silica shell can be easily controlled by changing reaction parameters (modified Stöber method).

■ Silica coatings have high drug absorption due to their high surface area and high pore volume.

■ Biocompatible.

The large pore volume of the silica shell makes them a desirable option for drug delivery applications. Many anticancer drugs on the market are poorly soluble and the use of mesoporous silica shell can be a good option for the easier transport of these drug molecules and reduced their side effects.[8,9] Silica pores do not work smart and the drug loaded on them begins to release as soon as they are placed in a physiological environment, whether healthy or tumor tissue (burst effect). The physiological pH of the body is 7.4 but may vary under different conditions (or locations) such as tumor tissues

[a]School of Metallurgy and Materials Engineering, Iran University of Science and Technology, P.O. Box 13114-16846, Tehran, Iran. E-mail: alamolhoda@iust.ac.ir; Fax: +98 2177240480; Tel: +98 2173228885

[b]Research Laboratory of Green Organic Synthesis & Polymers, Department of Chemistry, Iran University of Science and Technology, P.O. Box 13114-16846, Tehran, Iran

† Electronic supplementary information (ESI) available: XRD pattern of samples, N_2 adsorption/desorption, TGA analysis. See DOI: 10.1039/d0ra06916g

(pH $\sim$ 6.7–7.1) and lysosome (pH $\sim$ 5–5.5).[10–12] Smart systems are one of the most promising systems in the field of targeted drug delivery. Under special environmental conditions (such as pH) smart systems respond differently.[13–15] Chitosan is one of the natural polymers used in pH response systems and has a high biocompatibility that makes it suitable for biomedical applications. Chitosan is a natural polysaccharide which is used in many applications such as drug delivery, tissue engineering and wound dressing. Chitosan is one of the natural polymers with special properties such as antimicrobial, antioxidant and *etc.*[16–18]

One of the attractive applications of SPIONs is hyperthermia. By raising the temperature in tumor tissues up to 42–45 °C it is expected that the tumor cells die without harming healthy cells. SPIONs under alternating magnetic field can be used to reach the required temperature for hyperthermia.[19–21]

In this study, we designed a multifunctional carrier for drug delivery: silica as a drug reservoir, magnetite generates heat in the alternating magnetic field, and its chitosan coating prevents drug release into non-target tissues.

2.   Materials and methods

2.1.   Materials

Chitosan (medium molecular weight), ammonium hydroxide solution (28% NH_3 in H_2O) and glutaraldehyde solution (25% in H_2O) were obtained from Merck Inc. Sodium hydroxide, tetraethyl orthosilicate (TEOS), iron chlorides (Fe^{2+} and Fe^{3+}), and cetyl trimethylammonium bromide (CTAB) were purchased from Sigma Aldrich (USA). The materials were used without any further purification. Tamoxifen was purchased from Iran Hormone Company (Iran).

2.2.   Synthesis of oleic acid coated iron oxide

Co-precipitation of iron salts was used to synthesize magnetite. The deionized water was bubbled under nitrogen gas for 20 min to remove dissolved oxygen. Iron salts were added to deionized water at a molar ratio of $Fe^{3+}/Fe^{2+} = 2:1$. The mixture was stirred for 30 minutes by ultrasonic bath. The 1.1 M NaOH solution was added dropwise to the salt mixture and the black precipitate began to form. The reaction mixture was under a nitrogen atmosphere. Sodium hydroxide was added until pH reached $\sim$13. The mixture was stirred for 30 minutes and then heated to 75 °C for 15 minutes. Subsequently, oleic acid was added dropwise to iron oxide precipitates (oleic acid (OA) was used to prevent agglomeration and stability of iron oxide particles). The mixture was stirred for another 4 hours and the temperature was fixed at 75 °C. Then the precipitates were collected by centrifugation at 5400 rpm for 15 minutes and washed several times with deionized water. The precipitates were dispersed in deionized water and stored at 4 °C.

2.3.   Synthesis of amorphous silica thin layer

First, 1 g of SPIONs were added to 80 ml of ethanol, 20 ml of DI and ammonia solution (28%). The mixture was stirred for 20 minutes in an ultrasonic bath for complete dispersion of the particles. The tetraethyl orthosilicate (TEOS) was added dropwise (up to 2.5 ml) to the mixture and stirred for 8 hours. After this time, the particles were separated from the solution by a magnet and washed with DI water. The particles were dried at 55 °C for 12 h.

2.4.   Synthesis of mesoporous silica shell

First, 0.6 g of SPIONs was added to a solution containing 120 ml of ethanol and 3.5 ml of ammonia (28%) and placed in an ultrasonic bath for 30 minutes to completely disperse the particles (mixture 1). 2.5 g of CTAB was added to 160 ml of deionized water and placed in an ultrasonic bath for 10 minutes to obtain a homogeneous solution (mixture 2). Then, mixture (2) was slowly added to mixture (1) and stirring continued for 4 h. After this time, TEOS was added dropwise (up to 3.4 g) and stirred at room temperature for 8 h, then stirred at 70 °C for another 4 h. The particles were collected by magnet and washed with DI water. The particles were dried for 12 h at 55 °C. To remove CTAB, the particles were heated at 550 °C for 5 h.

2.5.   Synthesis of chitosan hydrogel

First, 0.5 g of Magnetite Mesoporous Silica Nanoparticles (MMSN) was dissolved in 25 ml of acetic acid (3%, v/v) and placed in an ultrasonic bath for 5 minutes to obtain a homogeneous mixture. Then, 0.5 g of chitosan (medium molecular weight) and 25 ml of acetic acid (3%, v/v) were added to the mixture and placed in an ultrasonic bath for 5 minutes (mixture 1). 0.4 ml glutaraldehyde was dissolved in 5 ml of acetic acid solution (3%, v/v) (mixture 2). Mixture (2) was added dropwise to the mixture (1). The mixture was stirred for 24 hours. The final product is a blackish brown gel due to the presence of MMSN particles. Then, the 6 M NaOH solution was slowly added to the gel for 1 h to neutralize the acidic solution. The gels were insoluble in neutral solution and easily separated by vacuum filtration and washed several times with ethanol. The resulting gel was divided into smaller sections and dried at room temperature.

2.6.   Drug loading and release

Phosphate-buffered saline (PBS) (pH 7.4) was used to load the drug into MMSN particles. The drug studied was tamoxifen. Tamoxifen (TMX) is used in the treatment of breast cancer. MMSN particles were added to PBS solution (pH 7.4) containing 1 mg ml^{-1} of the drug. The mixture was placed in an ultrasonic bath for 30 minutes then stirred with a magnetic stirrer for another 24 hours. After this time, the particles were collected by centrifugation at 8000 rpm for 10 minutes and washed several times with PBS to remove uncharged drug. PBS solution (pH 5, 7.4) was used to determine drug release. The drug release study was performed for 72 hours. To determine drug release, at specific times, 5 ml of supernatant was poured into a Falcon tube and centrifuged at 8000 rpm for 20 minutes. Ultraviolet-visible spectroscopy (at 278 nm) was used to determine the concentration of the unknown drug solution. Determination of drug release for each sample was repeated 3 times and standard deviation was determined for each profile.

2.7. *In vitro* study of hyperthermia

Alternating magnetic field (frequency = 315 kHz, intensity = 14.2 kA m^{-1}) was used to study hyperthermia samples. The study was performed for MMSN particles and chitosan hydrogels. At first, a concentration of 15 mg ml^{-1} was prepared from the samples. The samples were placed in a suitable location and a magnetic field was applied. Temperature/time changes were recorded by computer.

2.8. Cellular assay

In this study, 3-(4,5-dimethylthiazol-2-yl)-2,5-diphenyltetrazolium bromide (MTT) assay was used to evaluate the biocompatibility of MMSN/chitosan hydrogels. The murine fibroblast cell line (L929, Pasteur Institute, Tehran, Iran) was used for this evaluation. 10 000 cells per well were incubated with 150 μl of medium in 96-well plates for 24 h (medium was DMEM containing 10% FBS, incubation conditions was $CO_2 = 5\%$, $T = 37$ °C). After this time, 100 μl of the sample was added to cell wells and the cells were incubated for 24, 48 and 72 h treatment. A medium without any sample was used as control. After treatment, 100 μl of MTT (0.5 mg ml^{-1}) was added to the cells and incubated for 4 h. Then, Isopropyl alcohol was added to cells for dissolve formazan (for 20 min). ELISA (STAT FAX 2100, USA) was used to determine the concentration of wells (at 545 nm).

2.9. Characterization method

X-ray diffraction (XRD, PHILIPS, PW1730) was used to investigate the crystalline properties of the samples. The samples were dried in oven at 55 °C for 24 h before analysis. The FTIR spectra of the samples were obtained from a Shimadzu spectrometer (Thermo, AVATAR, USA). Transmission electron microscopy (TEM, PHILIPS, CM120) and scanning electron microscope (SEM, TESCAN, Vega II) was used to investigate the morphology and size of the samples. To prepare the samples, they were dispersed in an ultrasonic bath for 30 minutes, then a drop was poured onto the copper grid. TEM operating at 100 kV. Thermogravimetric analysis (TGA, Bahr, STA 504) was used to evaluate the thermal behavior of the samples. To investigate the hyperthermia of the samples (*in vitro*), an alternating magnetic field ($f = 315$ kHz, field intensity = 14.2 kA m^{-1}) was used. VSM analysis (at room temperature and field of 15 000 oersteds) was used to determine the magnetization of the samples (Meghnatis Daghigh Kavir Co., Kashan, Iran). Brunauer–Emmett–Teller (BET, BEL, BELSORP MINI II) analysis was used to determine the specific surface area of the samples. The pore size distribution curves were determined using the Barrett, Joyner, and Halenda (BJH) method. Ultraviolet-visible spectroscopy (UV/VIS, Shimadzu, Mini 1240 single beam) was used to determine the concentration of unknown solutions.

3. Results and discussion

Simultaneous use of chemotherapy and hyperthermia can improve cancer treatment, so hydrogel containing MMSNs were used in this study. Schematic representation of the hydrogel synthesis steps is shown in Fig. 1. Magnetite nanoparticles were used as agents that could cause magnetic manipulation and hyperthermia. Magnetite nanoparticles were synthesized by co-precipitation method and coated with a very thin oleic layer to stabilize and prevent agglomeration.[22] The silica coating was prepared using the modified Stöber method. Glutaraldehyde cross-linker was used to prepare chitosan hydrogel.

The SEM image of oleic acid-modified magnetite nanoparticles shows that the nanoparticles have a spherical morphology and a narrow size distribution, with an estimated size of about 20–30 nm (Fig. 2(a)). The SEM and TEM image clearly shows the spherical morphology of the magnetite mesoporous silica nanoparticles. The average size of MMSNs is about 150–160 nm, which is suitable for biomedical applications[23] (Fig. 2(b–d)). In the TEM image, presence of the iron oxide particles in the structure of MMSN was clearly visible (Fig. 2(g)). The SEM image of the hydrogel also shows the presence of new coating on the surface of the nanoparticles. It could be observed that due to the high adhesion of chitosan, the nanoparticles are not well separated (Fig. 2(e)). TEM images also confirm the presence of a chitosan coating on the surface of the MMSNs (Fig. 2(f–i)). The hydrogel showed good stability over a period of 6 months (this is longer than coatings like PEGF[24]) and no precipitation was observed which could be due to their hydrogel properties. The prepared hydrogel have unique properties such as drug delivery and response to stimuli such as pH, temperature, and magnetic field (for hyperthermia and magnetic manipulation) that make them novel among other coatings (these properties of hydrogels have been investigated). Fig. 3 shows a schematic illustration of the proposed mechanism for the formation of chitosan hydrogel with glutaraldehyde cross-linkers.[25,26]

3.1. Characterization of MMSN nanoparticles (FTIR)

FTIR analysis was used to investigate the surface modification of magnetite nanoparticles with oleic acid and their coating
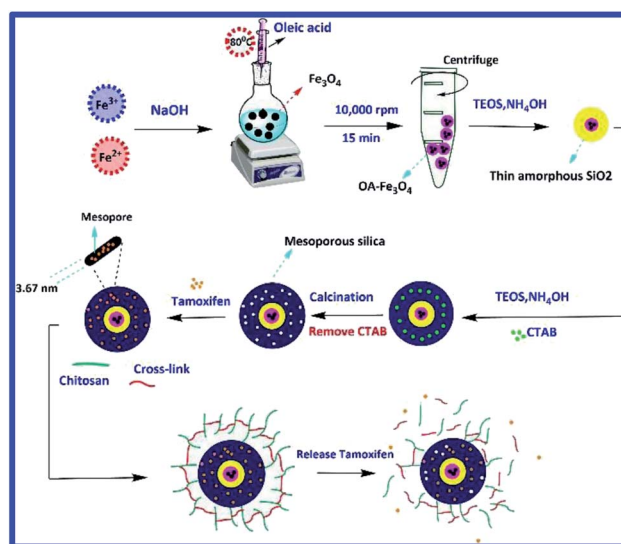

Fig. 1 Step by step schematic illustration of synthesis magnetite mesoporous silica nanoparticles and coating with chitosan for use as drug carrier (release was studied under different pH and temperature conditions).
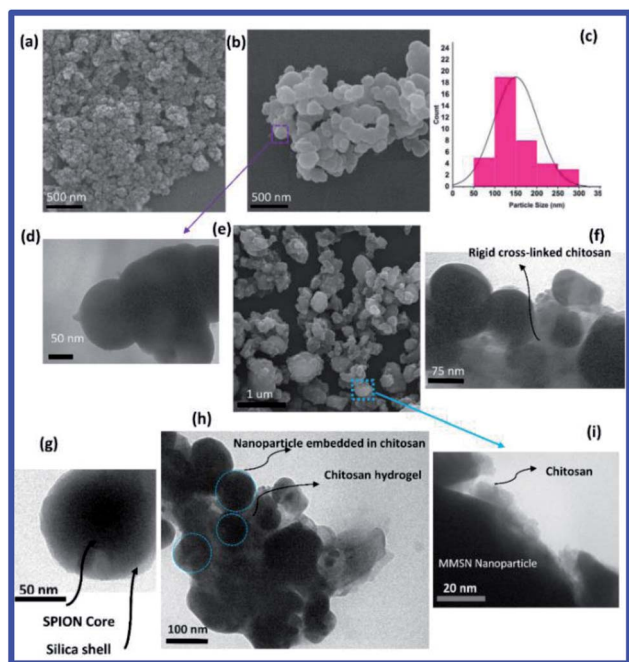
Fig. 2 (a) SEM image for OA-Fe$_3$O$_4$ nanoparticles (b) SEM image of MMSN nanoparticles, (c) size distribution histogram for MMSNs (d and g) TEM image of selected MMSN particles (e) SEM image of MMSN@chitosan hydrogel (f and h) TEM image of the MMSN/chitosan hydrogel at different magnifications (i) is a selective particle of MMSN/chitosan hydrogel that illustrates how the chitosan chain is bound by glutaraldehyde during the hydrogel process.
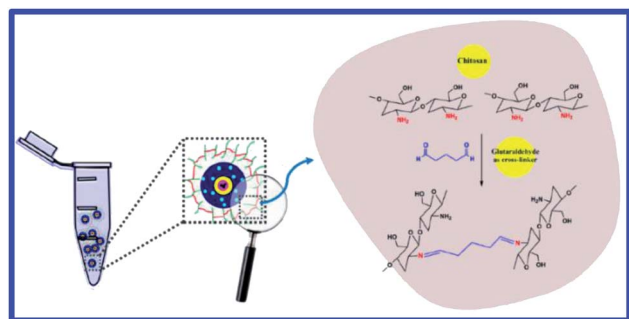

Fig. 3 Schematic illustration of chitosan hydrogel cross-linked by glutaraldehyde.
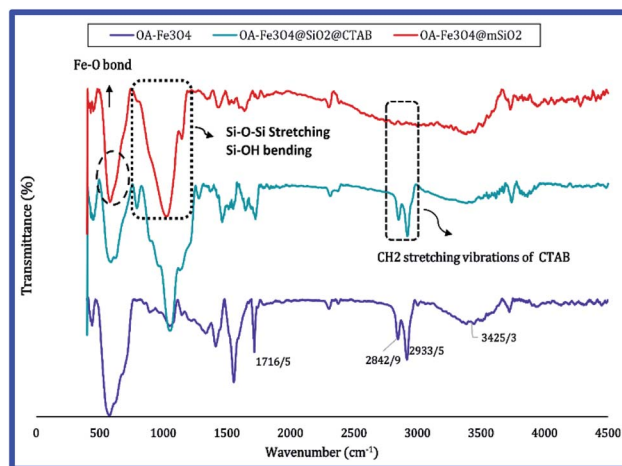

Fig. 4 FTIR spectra of OA-Fe$_3$O$_4$ nanoparticles, MMSN nanoparticles before calcination (with CTAB) and MMSN nanoparticles after calcination (without CTAB).

stretching vibration of mesoporous silica surface groups.[27] In the FTIR spectra of the MMSNs before calcination, the vibrations of CH$_2$ group of CTAB can be clearly seen at 2858 cm^{-1} and 2925 cm^{-1}, whereas these absorption bands are lost after calcination indicating the successful removal of CTAB from the structure.[28]

3.2. FTIR spectra of hydrogel

FTIR spectra of the chitosan, the magnetite mesoporous silica nanoparticle (MMSN) and the chitosan hydrogel are shown in Fig. 5. As could be observed in the FTIR spectrum of the chitosan hydrogel, the absorption band at 3456 cm^{-1} is related to the OH group in the chitosan (FTIR spectra of chitosan) which becomes less wider in the hydrogel and has shifted from 3456 cm^{-1} to 3411 cm^{-1} which can be attributed to the reduction of hydrogen bonds in the hydrogel.[29] The absorption band

with mesoporous silica (Fig. 4). The peak at 580 cm^{-1}, which is visible in all samples, indicates Fe–O bonding and confirms the presence of magnetite in the sample structure. The absorption bands at 3425 cm^{-1}, 2933 cm^{-1}, 2842 cm^{-1}, 1716 cm^{-1} and 1286 cm^{-1} corresponding to vibrations of the OH group, asymmetric and symmetric CH$_2$ stretch, stretch vibrations C=O group, and C–O stretch, respectively. All of these peaks are related to oleic acid, which confirms the presence of oleic coating on the surface of magnetite nanoparticles. The absorption band at 455 cm^{-1} refers to Si–O–Si bending vibrations. The peak at 987 cm^{-1} is related to the vibrations of Si–OH while the broad band at 1062 cm^{-1} corresponds to Si–O–Si
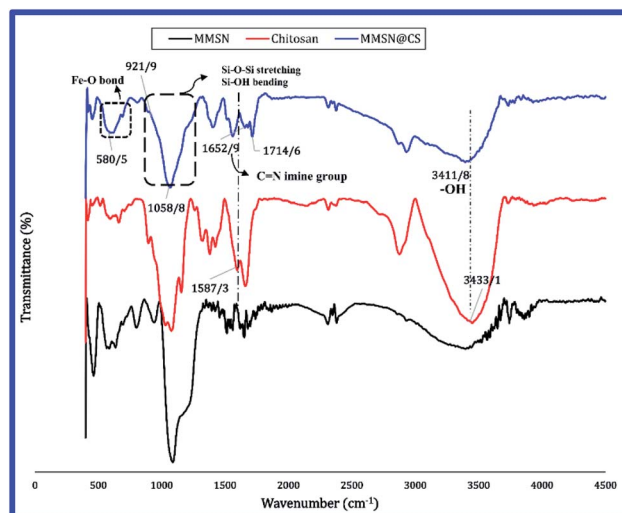

Fig. 5 FTIR spectra of MMSN, chitosan and MMSN@chitosan hydrogel.

at 3411 cm^{-1} indicates the vibration of OH and NH$_2$ groups in chitosan which cannot be separated due to the overlap. The band at 2900 cm^{-1} is related to the CH stretch vibration. In chitosan bulk due to the large amount of OH group its absorption band (at 3411 cm^{-1}) is intense and wide. A new peak is observed at 3411 cm^{-1} in the hydrogel, which represents which represents C=O group; due to the self-polymerization of glutaraldehyde to form large cross-linking chains.[30] During the process of preparing hydrogel, chitosan amino groups cross-linked and form imine groups (Fig. 5). The removal of the peak at 1587 cm^{-1} in the FTIR spectrum of hydrogel and the appearance of a new peak at 1652 cm^{-1} indicate the removal of NH$_2$ bands and formation of C=N (imine) bands, which demonstrates the success of the chitosan hydrogel processing.[31] The absorption band at 580 cm^{-1} is related to the Fe–O bond, and the peaks at 921 cm^{-1} and 1058 cm^{-1} represent Si–OH and Si–O–Si groups, which confirms presence of silica nanoparticles in the hydrogel.

3.3. X-ray diffraction pattern

Phase identification was performed using X-ray diffraction (XRD). Fig. S1(a)† shows the XRD pattern of magnetite nanoparticles, the diffraction pattern obtained from Fe$_3$O$_4$ nanoparticles shows very good agreement with the magnetite reference card (Fe$_3$O$_4$, reference card JCPDS No. 82-1533). The diffraction peaks at $2\theta \sim 30.1°$, 35.6°, 43.3°, 53.5°, 57.2° and 62.4° are related to crystalline planes (220), (311), (400), (422), (511) and (440), respectively. The absence of (300) and (210) peaks confirms that maghemite (γ-Fe$_2$O$_3$) is not formed during synthesis, so we have pure magnetite.[32] The diffraction pattern obtained from Fe$_3$O$_4$ nanoparticles shows very good agreement with the magnetite reference card (Fe$_3$O$_4$, reference card JCPDS No. 82-1533). In the XRD pattern of the MMSN, the broad diffraction peak at $2\theta \sim 20.9°$, indicates presence of amorphous silica. Also, the peaks of the magnetite nanoparticles can be clearly seen in the XRD pattern of the MMSN nanoparticles.

3.4. Vibrating-sample magnetometer (VSM)

To investigate the magnetization of the samples, VSM analysis was used at field of 15 000 Oe. The magnetization curves of the iron oxide, oleic acid-modified iron oxide, magnetite mesoporous silica nanoparticles (MMSN), and MMSN@chitosan hydrogel are shown in Fig. 6. The synthetic Fe$_3$O$_4$ nanoparticles are superparamagnetic because they do not have any remanence in their magnetization curve. According to previous reports, the theoretical saturation magnetization for bulk magnetite is $\sim$92 emu g^{-1} but as shown in the magnetite curve (Fig. 6) this value is $\sim$59.8 emu g^{-1} which can be due existence of noncollinear spins at the surface of magnetite.[33,34] The saturation magnetizations obtained from the VSM analysis for the other samples are summarized in Table 1.

The obtained values for saturation magnetization of magnetite nanoparticles before and after surface modification are in consistent with the results of other researches.[34,35] Modifying the surface of the magnetite nanoparticles with different coatings (oleic acid, mesoporous silica and chitosan
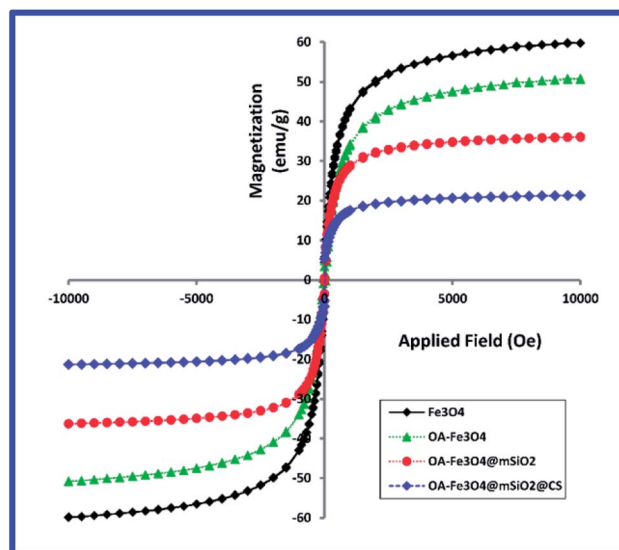

Fig. 6 Magnetization results for magnetite, OA-Fe$_3$O$_4$, magnetite mesoporous silica nanoparticles (MMSN) and MMSN@chitosan hydrogel (measured at 15 000 Oe and room temperature).

hydrogel) the saturation magnetization (M_s) decreases and M_s reaches its lowest value in the hydrogel.

This decrease in saturation magnetization can be attributed to the replacement of Fe$_3$O$_4$ magnetic with a silica and chitosan non-magnetic which results in decreasing of the amount of magnetite in MMSNs and chitosan hydrogel. Also when magnetite nanoparticles are embedded in chitosan hydrogel (cross-linked with glutaraldehyde) their alignment along their easy axis would not be easy. This can also reduce the saturation magnetization.[24,34]

For biomedical applications such as drug delivery and hyperthermia a saturation magnetization of $\sim$8–19 emu g^{-1} is required which according to VSM results the synthesized MMSNs@chitosan hydrogel are useful for biomedical applications.[32,35,36]

3.5. Pore characteristics of MMSN particle

BET analysis was performed for characterization of magnetite mesopores silica nanoparticles (MMSN) before and after drug loading. The nitrogen absorption–desorption isotherm and pore size distribution curve for MMSN and MMSN@TMX is shown in Fig. S2 and S3.† As shown in Fig. S2(a) and S3(a),† the isotherm curve of the MMSN and MMSN@TMX particles are IV type isotherm curve in IUPAC classification which represents

Table 1 The saturation magnetization values of the samples under 15 000 Oe at room temperature

Sample	M_s (emu g^{-1})
Fe$_3$O$_4$	59.8
OA-Fe$_3$O$_4$	50.7
Magnetite mesoporous silica nanoparticles (MMSN)	36.1
MMSN@chitosan hydrogel	21.3

the mesoporous structures. Therefore, the presence of mesopore in MMSN and MMSN@TMX particles is confirmed. Both types of mesoporous–macroporous porosities were observed in the pore distribution curve and the adsorption and desorption isotherms of nanoparticles (Fig. S2(a, b) and S3(a, b)†). The characteristic porosity of samples such as average pore size (calculated by BJH method), total pore volume, and BET surface area are presented in Table 2.

3.6. Thermogravimetric analysis (TGA)

Thermal properties of hydrogel and MMSNs before and after drug loading were determined using thermo-gravimetric analysis (TGA) to obtain information as thermal stability, cross-linking content of hydrogel and organic groups in the structure (presence of chitosan coating).[37] Fig. S4† shows the TGA results for MMSN before and after drug loading and MMSN@chitosan hydrogel (up to 800 °C at a heating rate of 10 °C min^{-1} in air). As shown in Fig. S4,† the uncoated MMSNs do not show significant weight loss except in the range below 200 °C which is due to physically absorbed water. The drug-loaded MMSN particles showed a 8% weight loss compared to MMSN without drug which can be attributed to tamoxifen. Decomposition behavior of the hydrogel can be divided into three stages. The first stage occurs at temperatures of 50–185 °C and a ∼5% weight loss is observed, which is due to the evaporation of the physical water molecules of the hydrogel. In the second stage ∼15% weight loss is observed at temperature of 210–350 °C which can be attributed to the degradation of hydroxyl group of the chitosan backbone chain. The third stage which occurs at the temperature range of 360–520 °C is due to structural degradation of chitosan main chain and crosslinkers (glutaraldehyde).[30,32,38] TGA analysis indicates that chitosan hydrogel with glutaraldehyde cross-linkers have been successfully formed.

3.7. In vitro hyperthermia

The results of hyperthermia analysis of the samples are shown in Fig. 7. Samples were dispersed in physiological saline at a concentration of 15 mg ml^{-1} and subjected to alternating magnetic field. For the application of hyperthermia, radio frequencies in the range of kHz to MHz are used.[39,40] Therefore, in this study, a frequency of 315 kHz and intensity 14.3 kA m^{-1} was chosen for a period of 15 minutes. The temperature change for MMSN nanoparticle and chitosan hydrogel are 25 → 70 °C and 25 → 58 °C, respectively. The time required to reach the optimum temperature for hyperthermia (43 °C) for MMSN and chitosan hydrogel is 3 and 5 min, respectively. The longer time to reach the desired temperature for the hydrogel can be attributed to the non-magnetic coating of chitosan on the
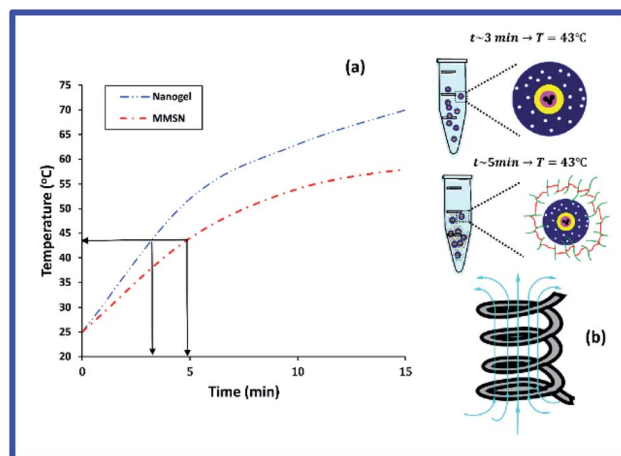

Fig. 7 (a) Curve of temperature changes obtained from hyperthermia (in vitro) for MMSNs and MMSN@chitosan hydrogel dispersed in physiological saline with a concentration of 15 mg ml^{-1} under an alternating magnetic field (f = 315 kHz and intensity = 14.3 kA m^{-1}). (b) Schematic illustration of magnetic coil and field lines inside it.

nanoparticles, which makes the nanoparticles unable to orient in their easy axis which reduces the saturation magnetization and prolongs the heat generation process by the nanoparticles. Chitosan hydrogel have the ability to generate heat for hyperthermia in a short period of time, so their heat generation characteristic can be used for hyperthermia application. The following equation which is related to specific absorption rate (SAR) can be used to calculate the heat capacity of MMSN nanoparticles and hydrogel:[41]

$$\text{SAR(w/g)} = \frac{C_w}{m} \frac{\Delta T}{\Delta t} \qquad (2)$$

where C_w corresponds to the solution heat capacity (due to the low concentration of the samples, neglecting their heat capacity so $C_w \sim C_{ps} \sim 4139 \text{ J kg}^{-1} \text{ °C}^{-1}$),[42] $\Delta T/\Delta t$ is the slope of the curve in the first seconds (up to 60 seconds). m is total amount of MMSN in solution (solution = MMSN + physiological saline). The SAR values for MMSN nanoparticles and chitosan hydrogel are 76.2 w/g and 108.6 w/g, respectively. Comparison of the results with previous reports indicates that chitosan hydrogel is useable in hyperthermia applications.[36]

3.8. In vitro drug release

pH is one of the key parameters in drug release because. Temperatures of 42–45 °C can cause apoptosis of cancer cells without damaging healthy tissue.[20,44] The in vitro drug release from MMSN@chitosan hydrogel was determined in two media with different pH values (pH 7.4 and 5) to simulate the physiological condition and tumor intracellular microenvironment and two different temperatures (37 °C and 43 °C) to simulate physiological body temperature and hyperthermia temperature which caused cancer cell death. Fig. 8 shows the drug release of the samples within 72 hours. The cumulative amounts of drug released within 72 h from TMX/MMSN@chitosan hydrogel samples at pH 7.4 and temperatures of 37 °C and 43 °C are 15.6% and 29.1%, respectively which vary slightly. The hydrogel

Table 2 Pore characteristics of magnetic mesoporous silica nanoparticles

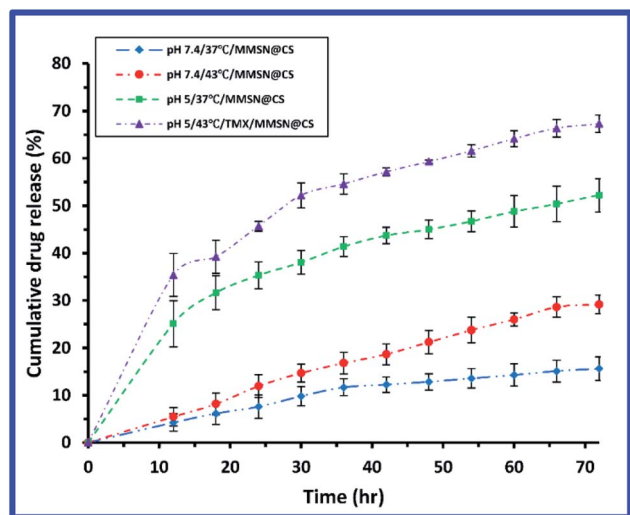| Sample	BET surface area (m^2 g^{-1})	Pore volume (cm^3 g^{-1})	Pore size (nm)
MMSN	745.2	0.62	3.67
MMSN@TMX	436.8	0.34	2.51

Fig. 8 Curve of drug release from MMSN@chitosan hydrogel at different pH and temperatures over 72 h.
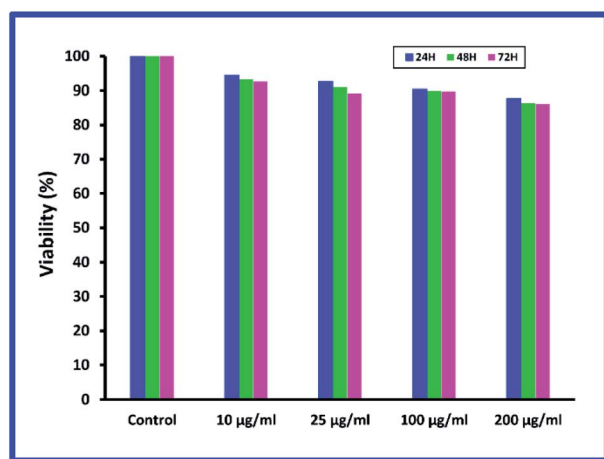

Fig. 9 Cellular biocompatibility results (MTT) for MMSN@chitosan hydrogel on L929 cells for 24, 48 and 72 h treatment.

release about 52.2% and 67.3% of the loaded tamoxifen over a 72 h period at pH 5.0 and temperature of 37 °C and 42 °C, respectively. The increase in drug release at pH 5.0 compared to pH 7.4 is due to sensitivity of chitosan to pH. Comparing the results of drug release from hydrogel (regardless of the temperature parameter) with previous research shows that glutaraldehyde cross-linkers have reduced the burst effect about 25–65% due to glutaraldehyde cross-links and the swelling properties of the hydrogel which prevent burst release.[43–45]

A schematic illustration of the circulation of chitosan hydrogel in body to reach the cell and release of drug is shown in Fig. S5.†

3.9. MTT assay

Biocompatibility is one of the key parameters for biomedical applications. Systems designed for applications such as drug delivery should not exhibit significant toxicity; therefore, the

MTT assay was used to evaluate synthetic hydrogel. The results of cell biocompatibility (MTT) for chitosan hydrogel are shown in Fig. 9. Cellular evaluation was performed on L929 cells and 24, 48 and 72 h treatment and different concentrations. The cell viability of hydrogel at different concentrations was acceptable and no effective toxicity was observed. Cell viability of hydrogel is greater than 80% (after 72 h). The synthesized hydrogel is safe and can be used for drug delivery.

4. Conclusions

SPIONs were synthesized by co-precipitation, and their surface was modified with a mesoporous silica shell to enhance biocompatibility and subsequently chitosan was used to prevent burst effect and drug release into non-target chitosan tissue. In this study, MMSN/chitosan hydrogel was investigated for drug delivery and hyperthermia. Drug release studies over a period of 72 hours show that hydrogels release different amounts tamoxifen under different pH and temperature conditions and most release occurs at pH 5.0 (pH simulation in endosomes) and 43 °C (temperature required for hyperthermia). The study of *in vitro* hyperthermia of hydrogel and MMSNs shows that the temperature rise in MMSNs is much higher than that of hydrogels, which could be due to the non-magnetic coating of MMSNs in hydrogel but the hydrogel can provide the necessary heat for hyperthermia at approximately 5 minutes which is a reasonable time according to previous reports. The cell biocompatibility of hydrogel was determined by MTT assay. The results showed that the hydrogel was not toxic at the studied durations and concentrations and it can be concluded that any cell death resulting from the MMSN/chitosan hydrogel will be due to the release of the toxic drug (tamoxifen).

Conflicts of interest

There are no conflicts to declare.

Acknowledgements

References

1 M. Mahmoudi, S. Sant, B. Wang, S. Laurent and T. Sen, Superparamagnetic iron oxide nanoparticles (SPIONs): development, surface modification and applications in chemotherapy, *Adv. Drug Delivery Rev.*, 2011, **63**(1–2), 24–46.

2 S. Laurent, A. A. Saei, S. Behzadi, A. Panahifar and M. Mahmoudi, Superparamagnetic iron oxide nanoparticles for delivery of therapeutic agents: opportunities and challenges, *Expert Opin. Drug Delivery*, 2014, **11**(9), 1449–1470.

3 M. Arruebo, R. Fernández-Pacheco, M. R. Ibarra and J. Santamaría, Magnetic nanoparticles for drug delivery, *Nano Today*, 2007, **2**(3), 22–32.

4 N. Tran and T. J. Webster, Magnetic nanoparticles: biomedical applications and challenges, *J. Mater. Chem.*, 2010, **20**(40), 8760–8767.

5 L. H. Reddy, J. L. Arias, J. Nicolas and P. Couvreur, Magnetic nanoparticles: design and characterization, toxicity and biocompatibility, pharmaceutical and biomedical applications, *Chem. Rev.*, 2012, **112**(11), 5818–5878.

6 I. I. Slowing, J. L. Vivero-Escoto, C.-W. Wu and V. S.-Y. Lin, Mesoporous silica nanoparticles as controlled release drug delivery and gene transfection carriers, *Adv. Drug Delivery Rev.*, 2008, **60**(11), 1278–1288.

7 N. Zhu, H. Ji, P. Yu, J. Niu, M. Farooq, M. W. Akram, I. Udego, H. Li and X. Niu, Surface modification of magnetic iron oxide nanoparticles, *Nanomaterials*, 2018, **8**(10), 810.

8 N. Ž. Knežević, E. Ruiz-Hernández, W. E. Hennink and M. Vallet-Regí, Magnetic mesoporous silica-based core/shell nanoparticles for biomedical applications, *RSC Adv.*, 2013, **3**(25), 9584–9593.

9 I. I. Slowing, B. G. Trewyn, S. Giri and V. Y. Lin, Mesoporous silica nanoparticles for drug delivery and biosensing applications, *Adv. Funct. Mater.*, 2007, **17**(8), 1225–1236.

10 B. A. Webb, M. Chimenti, M. P. Jacobson and D. L. Barber, Dysregulated pH: a perfect storm for cancer progression, *Nat. Rev. Cancer*, 2011, **11**(9), 671–677.

11 E. Persi, M. Duran-Frigola, M. Damaghi, W. R. Roush, P. Aloy, J. L. Cleveland, R. J. Gillies and E. Ruppin, Systems analysis of intracellular pH vulnerabilities for cancer therapy, *Nat. Commun.*, 2018, **9**(1), 1–11.

12 M. J. Geisow and W. H. Evans, pH in the endosome: measurements during pinocytosis and receptor-mediated endocytosis, *Exp. Cell Res.*, 1984, **150**(1), 36–46.

13 M. Manzano and M. Vallet-Regí, New developments in ordered mesoporous materials for drug delivery, *J. Mater. Chem.*, 2010, **20**(27), 5593–5604.

14 C. Alvarez-Lorenzo and A. Concheiro, Smart drug delivery systems: from fundamentals to the clinic, *Chem. Commun.*, 2014, **50**(58), 7743–7765.

15 D. Liu, F. Yang, F. Xiong and N. Gu, The smart drug delivery system and its clinical potential, *Theranostics*, 2016, **6**(9), 1306.

16 M. M. Villar-Chavero, J. C. Domínguez, M. V. Alonso, M. Oliet and F. Rodriguez, Tuning the rheological properties of cellulosic ionogels reinforced with chitosan: The role of the deacetylation degree, *Carbohydr. Polym.*, 2019, **207**, 775–781.

17 R. Jayakumar, D. Menon, K. Manzoor, S. V. Nair and H. Tamura, Biomedical applications of chitin and chitosan based nanomaterials—A short review, *Carbohydr. Polym.*, 2010, **82**(2), 227–232.

18 M. S. Amini-Fazl, R. Mohammadi and K. Kheiri, 5-Fluorouracil loaded chitosan/polyacrylic acid/Fe_3O_4 magnetic nanocomposite hydrogel as a potential anticancer drug delivery system, *Int. J. Biol. Macromol.*, 2019, **132**, 506–513.

19 C. S. Kumar and F. Mohammad, Magnetic nanomaterials for hyperthermia-based therapy and controlled drug delivery, *Adv. Drug Delivery Rev.*, 2011, **63**(9), 789–808.

20 S. Laurent, S. Dutz, U. O. Häfeli and M. Mahmoudi, Magnetic fluid hyperthermia: focus on superparamagnetic iron oxide nanoparticles, *Adv. Colloid Interface Sci.*, 2011, **166**(1–2), 8–23.

21 T. Kobayashi, Cancer hyperthermia using magnetic nanoparticles, *Biotechnol. J.*, 2011, **6**(11), 1342–1347.

22 N. V. Jadhav, A. I. Prasad, A. Kumar, R. Mishra, S. Dhara, K. Babu, C. Prajapat, N. Misra, R. Ningthoujam and B. Pandey, Synthesis of oleic acid functionalized Fe_3O_4 magnetic nanoparticles and studying their interaction with tumor cells for potential hyperthermia applications, *Colloids Surf., B*, 2013, **108**, 158–168.

23 Q. He and J. Shi, Mesoporous silica nanoparticle based nano drug delivery systems: synthesis, controlled drug release and delivery, pharmacokinetics and biocompatibility, *J. Mater. Chem.*, 2011, **21**(16), 5845–5855.

24 M. Mahmoudi, A. Simchi, M. Imani and U. O. Hafeli, Superparamagnetic iron oxide nanoparticles with rigid cross-linked polyethylene glycol fumarate coating for application in imaging and drug delivery, *J. Phys. Chem. C*, 2009, **113**(19), 8124–8131.

25 L. Baldino, S. Concilio, S. Cardea, I. De Marco and E. Reverchon, Complete glutaraldehyde elimination during chitosan hydrogel drying by SC-CO_2 processing, *J. Supercrit. Fluids*, 2015, **103**, 70–76.

26 B. Cheng, B. Pei, Z. Wang and Q. Hu, Advances in chitosan-based superabsorbent hydrogels, *RSC Adv.*, 2017, **7**(67), 42036–42046.

27 F. Sevimli and A. Yılmaz, Surface functionalization of SBA-15 particles for amoxicillin delivery, *Microporous Mesoporous Mater.*, 2012, **158**, 281–291.

28 C. Wang, S. Tao, W. Wei, C. Meng, F. Liu and M. Han, Multifunctional mesoporous material for detection, adsorption and removal of Hg^{2+} in aqueous solution, *J. Mater. Chem.*, 2010, **20**(22), 4635–4641.

29 S. W. Ali, S. Rajendran and M. Joshi, Synthesis and characterization of chitosan and silver loaded chitosan nanoparticles for bioactive polyester, *Carbohydr. Polym.*, 2011, **83**(2), 438–446.

30 Z. A. Sutirman, M. M. Sanagi, K. J. A. Karim and W. A. W. Ibrahim, Preparation of methacrylamide-functionalized crosslinked chitosan by free radical polymerization for the removal of lead ions, *Carbohydr. Polym.*, 2016, **151**, 1091–1099.

31 D. Y. Pratt, L. D. Wilson and J. A. Kozinski, Preparation and sorption studies of glutaraldehyde cross-linked chitosan copolymers, *J. Colloid Interface Sci.*, 2013, **395**, 205–211.

32 S. Kayal and R. Ramanujan, Doxorubicin loaded PVA coated iron oxide nanoparticles for targeted drug delivery, *Mater. Sci. Eng., C*, 2010, **30**(3), 484–490.

33 L. Harris, J. Goff, A. Carmichael, J. Riffle, J. Harburn, T. St. Pierre and M. Saunders, Magnetite nanoparticle dispersions stabilized with triblock copolymers, *Chem. Mater.*, 2003, **15**(6), 1367–1377.

34 A. K. Gupta and M. Gupta, Synthesis and surface engineering of iron oxide nanoparticles for biomedical applications, *Biomaterials*, 2005, **26**(18), 3995–4021.

35 F. Wang, G. M. Pauletti, J. Wang, J. Zhang, R. C. Ewing, Y. Wang and D. Shi, Dual surface-functionalized Janus nanocomposites of polystyrene/Fe_3O_4@SiO_2 for simultaneous tumor cell targeting and stimulus-induced drug release, *Adv. Mater.*, 2013, **25**(25), 3485–3489.

36 M. S. Moorthy, Y. Oh, S. Bharathiraja, P. Manivasagan, T. Rajarathinam, B. Jang, T. T. V. Phan, H. Jang and J. Oh, Synthesis of amine-polyglycidol functionalised Fe_3O_4@SiO_2 nanocomposites for magnetic hyperthermia, pH-responsive drug delivery, and bioimaging applications, *RSC Adv.*, 2016, **6**(111), 110444–110453.

37 L. Poon, L. D. Wilson and J. V. Headley, Chitosan-glutaraldehyde copolymers and their sorption properties, *Carbohydr. Polym.*, 2014, **109**, 92–101.

38 Y. Lin, L. Wang, J. Zhou, L. Ye, H. Hu, Z. Luo and L. Zhou, Surface modification of PVA hydrogel membranes with carboxybetaine methacrylate *via* PET-RAFT for anti-fouling, *Polymer*, 2019, **162**, 80–90.

39 A. Muela, D. Muñoz, R. Martin-Rodriguez, I. a. Orue, E. Garaio, A. Abad Diaz de Cerio, J. Alonso, J. A. Garcia and M. L. Fdez-Gubieda, Optimal parameters for hyperthermia treatment using biomineralized magnetite nanoparticles: theoretical and experimental approach, *J. Phys. Chem. C*, 2016, **120**(42), 24437–24448.

40 H. Shoji, M. Motegi, K. Osawa, N. Okonogi, A. Okazaki, Y. Andou, T. Asao, H. Kuwano, T. Takahashi and K. Ogoshi, A novel strategy of radiofrequency hyperthermia (neothermia) in combination with preoperative chemoradiotherapy for the treatment of advanced rectal cancer: a pilot study, *Cancer Med.*, 2015, **4**(6), 834–843.

41 P. Shete, R. Patil, N. Thorat, A. Prasad, R. Ningthoujam, S. Ghosh and S. Pawar, Magnetic chitosan nanocomposite for hyperthermia therapy application: Preparation, characterization and *in vitro* experiments, *Appl. Surf. Sci.*, 2014, **288**, 149–157.

42 A. Blake, G. Petley and C. Deakin, Effects of changes in packed cell volume on the specific heat capacity of blood: implications for studies measuring heat exchange in extracorporeal circuits, *Br. J. Anaesth.*, 2000, **84**(1), 28–32.

43 X. Hu, Y. Wang and B. Peng, Chitosan-capped mesoporous silica nanoparticles as pH-responsive nanocarriers for controlled drug release, *Chem.–Asian J.*, 2014, **9**(1), 319–327.

44 A. Popat, J. Liu, G. Q. M. Lu and S. Z. Qiao, A pH-responsive drug delivery system based on chitosan coated mesoporous silica nanoparticles, *J. Mater. Chem.*, 2012, **22**(22), 11173–11178.

45 M. P. Daryasari, M. R. Akhgar, F. Mamashli, B. Bigdeli and M. Khoobi, Chitosan-folate coated mesoporous silica nanoparticles as a smart and pH-sensitive system for curcumin delivery, *RSC Adv.*, 2016, **6**(107), 105578–105588.